

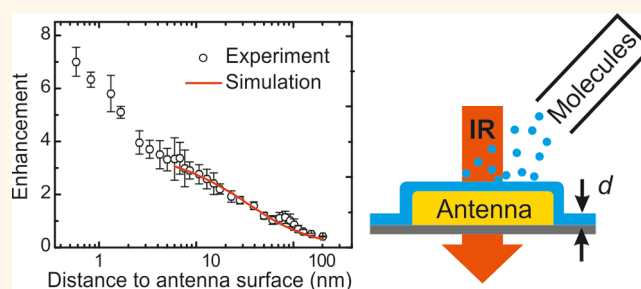
Spatial Extent of Plasmonic Enhancement of Vibrational Signals in the Infrared

Frank Neubrech,^{†,*,*} Sebastian Beck,^{*,§} Tobias Glaser,^{*,§} Mario Hentschel,^{†,‡} Harald Giessen,[†] and Annemarie Pucci^{*,§,⊥}

[†]4th Physics Institute and Research Center SCoPE, University of Stuttgart, Pfaffenwaldring 57, 70569 Stuttgart, Germany, [‡]Kirchhoff Institute for Physics, University of Heidelberg, Im Neuenheimer Feld 227, 69120 Heidelberg, Germany, [§]InnovationLab GmbH, Speyerer Straße 4, 69115 Heidelberg, Germany, and [⊥]Centre for Advanced Materials, University of Heidelberg, Im Neuenheimer Feld 227, 69120 Heidelberg, Germany. ^{*}Present address: Materials Science Division, Lawrence Berkeley National Laboratory, Berkeley, California 94720, United States.

ABSTRACT Infrared vibrations of molecular species can be enhanced by several orders of magnitude with plasmonic nanoantennas. Based on the confined electromagnetic near-fields of resonantly excited metal nanoparticles, this antenna-assisted surface-enhanced infrared spectroscopy enables the detection of minute amounts of analytes localized in the nanometer-scale vicinity of the structure. Among other important parameters, the distance of the vibrational oscillator of the analyte to the nanoantenna surface determines the signal enhancement. For sensing applications, this is

a particularly important issue since the vibrating dipoles of interest may be located far away from the antenna surface because of functional layers and the large size of biomolecules, proteins, or bacteria. The relation between distance and signal enhancement is thus of paramount importance and measured here with *in situ* infrared spectroscopy during the growth of a probe layer. Our results indicate a diminishing signal enhancement and the effective saturation of the plasmonic resonance shift beyond 100 nm. The experiments carried out under ultra-high-vacuum conditions are supported by numerical calculations.



KEYWORDS: plasmonics · nanoantennas · local near-field intensity · surface-enhanced infrared spectroscopy · organic molecules

In recent years surface-enhanced infrared (IR) absorption (SEIRA)¹ has gained tremendous attention because of the extraordinarily strong signal enhancement of more than 5 orders of magnitude when using resonant plasmonic antennas.^{2,3} Whereas several impressive results were obtained,^{4–10} many open problems still hamper its broad application in life sciences, medicine, food and water safety, or explosives detection. Some of these are related to the nanoantenna surface to which the molecules are adsorbed. It may happen that their vibrations do not appear even if the nanoantennas are properly designed and fabricated. One reason could be quantum effects,¹¹ as shown for small carbon monoxide molecules directly adsorbed on a gold antenna.¹² Other factors in practice could be impurities that hinder adsorption of the molecules of interest in the sites of the

plasmonic near-field enhancement, which are localized in nanometer-sized volumes.^{13,14} A further reason for missing antenna-enhanced infrared signals could be that damping is too strong and therefore the Fano effect, which is the underlying coupling mechanism for SEIRA, is not effective.¹⁵ Beyond these damping and surface effects, the enhancement of infrared vibrations of biomolecules depends on the adsorption geometry of the molecules (*e.g.*, ref 16). If the antennas are covered with layers that are too thick, the SEIRA effect may almost disappear, as derived from a comparison of antenna-enhanced signals of a 30 nm thick polymer layer¹⁷ and molecular films of only a few nanometers' thickness.^{9,12} For practical applications, the question of up to which distance can reasonable signal enhancement be expected is much more important than the interface problem

* Address correspondence to f.neubrech@pi4.uni-stuttgart.de.

Received for review March 28, 2014 and accepted May 8, 2014.

Published online May 08, 2014
10.1021/nn5017204

© 2014 American Chemical Society

since in most sensing applications the antenna is covered by a functional monolayer that already pre-selects the adsorbates (e.g., ref 18). From a purely numerical study¹⁹ it was already estimated that above a distance of approximately 100 nm the enhanced vibrational signals may vanish. However, an experimental proof of the relation between the signal enhancement and the distance starting from less than one nanometer up to more than 200 nm was not given.

In the present work, we address the distance problem by experimentally monitoring SEIRA while a molecular probe film is growing on an antenna array. Antenna-assisted SEIRA of well-known probe molecules allows mapping of plasmonic near-fields with a nanometer-scale resolution limited only by the size of the probe molecule, here 4,4'-bis(*N*-carbazolyl)-1,1'-biphenyl (CBP). We evaporated this material stepwise under ultra-high-vacuum (UHV) conditions onto gold nanostructures and acquired IR spectra after each evaporation step (Figure 1a). Besides the decreasing signal enhancement, we also studied the red-shift of the plasmonic resonance with increasing CBP thickness. This shift originates from the polarizability change caused by the evaporated material. Furthermore, we performed finite-difference time-domain (FDTD) simulations and found a very good qualitative agreement with our experimental data.

RESULTS AND DISCUSSION

It is well known that electromagnetic fields of metal nanoantennas are typically confined on the nanometer scale, resulting in near-field intensity enhancements up to 2000 (see Figure 1b), which can be calculated with nanometer precision employing simulation techniques, e.g., FDTD, boundary element,²⁰ or finite element²¹ algorithms. In order to experimentally achieve a similar resolution, which is required to vertically resolve the near-fields and thus the plasmonic enhancement, without using scattering near-field optical microscopy^{22,23} we covered the lithographic antennas with CBP, acting as probe molecules. CBP molecules, with typical dimensions of about $2 \times 1 \times 0.25 \text{ nm}^3$, enable such a thickness resolution in the nanometer range and modify the electronic structure of the antenna surface only marginally since they are physisorbed.²⁴ This allows us to exclude strong chemical effects, as may be present in surface-enhanced Raman scattering (SERS) (e.g., ref 25), and interpret our results with purely classical electromagnetic models. Furthermore, CBP features several vibrational bands, which in principle allow for multispectral analysis.²⁶ CBP layers freshly evaporated at room temperature are amorphous and thus isotropic in their optical properties.²⁴

In order to achieve an optimum coupling between the CBP vibrations and the plasmonic excitation, we employed electron beam lithography to fabricate

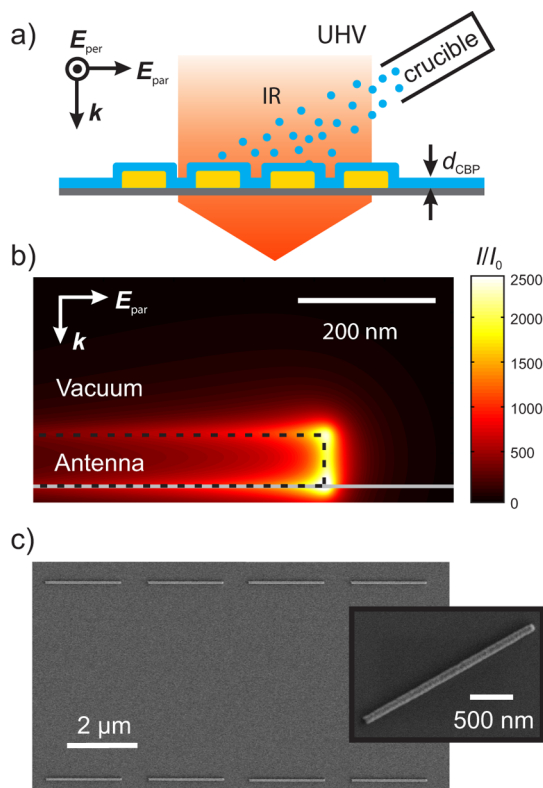


Figure 1. (a) Illustration of our experimental technique. Under UHV conditions gold nanoantennas (yellow bars) are covered stepwise with molecular CBP layers (blue) of different thickness (d_{CBP}) that act as near-field probes. After each evaporation step, corresponding to a certain thickness d_{CBP} , the infrared transmittance is recorded for both polarizations (E_{par} and E_{per}). (b) Numerically calculated electromagnetic near-field intensity ($I = |E_x|^2 + |E_y|^2 + |E_z|^2$) of a resonantly excited antenna (resonance frequency $\omega_{\text{res}} = 1632 \text{ cm}^{-1}$) recorded 6 nm away from the antenna's surface and normalized to the field distribution of the bare substrate I_0 . Only one apex range of the antenna is shown. The gray line indicates the substrate's surface. The geometric dimensions of the nanostructure (length $L = 2140 \text{ nm}$, width $w = 90 \text{ nm}$, and height $h = 80 \text{ nm}$, contour as dashed black line) are taken as the nanofabrication data. In the experiments, the antennas are arranged in a periodic array, as shown in the scanning electron micrograph in (c) (zoom).

structurally and spectrally tailored gold nanostructures on an infrared transparent calcium difluoride (CaF_2) substrate (see Methods). The antennas are arranged in a periodic array (Figure 1c) with lateral and longitudinal distances large enough to have only marginal antenna interaction⁹ in the spectral range of interest. Thus, the measured optical response can be considered as that of a single antenna in a first approximation. After the nanofabrication process, we stepwise evaporated distinct amounts of CBP onto the sample under UHV conditions, ensuring a homogeneous layer growth and stable conditions during the infrared spectroscopic measurements. The thickness of the CBP layer (d_{CBP}), whose precision is of paramount importance for our studies, was determined from the deposition time, and the rate was calibrated with a quartz microbalance.²⁴ Following this approach, over 30 layer thicknesses

ranging from 0.5 to 200 nm were evaluated. More details are given in the Methods section. Please note that due to the stochastic nature of the evaporation process, the thickness d_{CBP} is an average value. This is especially important for layer thicknesses smaller than the geometric dimensions of the molecules. After each evaporation step corresponding to a certain CPB layer thickness, relative transmittance measurements near normal incidence were performed for incident light polarized parallel and perpendicular to the antenna axis (Figure 1a). From these spectra we calculated the extinction, defined as $1 - (T/T_0)$, where T is the transmittance at the sample position, *i.e.*, the antennas covered with CBP, and T_0 is the reference measurement, *i.e.*, the antennas without CBP.

Typical extinction spectra of nanoantennas covered with CBP layers of selected thicknesses are shown in Figure 2 for parallel and perpendicular polarized infrared radiation.

For perpendicular polarization (shown in Figure 2a) strong absorption of C–N, C–C, and C–H vibrations is found between 1200 and 1650 cm^{-1} . With respect to their spectral positions and oscillator strengths, the measured vibrations are in good agreement with studies of CBP films grown on unstructured substrates (see Supporting Information). Thus, fits to our experimental spectra enable us to determine the layer thickness based on the CBP dielectric function taken from ref 26. The fitted layer thicknesses are in good agreement with the values obtained from the deposition time and rate and are therefore used in the following. However, the situation completely changes for parallel polarization. Here, the infrared optical response is dominated by the broadband plasmonic excitation of the antennas. In addition, we observe several narrow-band CBP vibrations. Each band observed in the measurement with parallel polarized light (Figure S1b) is a superposition of two vibrational signals originating from different sample areas. One part stems from the coupling with the antennas (Figure 2b) and features the characteristic asymmetric Fano-type line shape,^{15,27} whereas the other part originates from molecules located sufficiently far apart from the enhanced plasmonic near-fields, namely, the area between the antennas (Figure 2a). Since we are interested only in the enhanced vibrational signal, we divide the spectra measured with parallel polarized light by the respective ones under perpendicular polarization and obtain the purely antenna-enhanced CBP vibrational signals (Figure 2b). As expected, these signals are enhanced, show an asymmetric Fano-type line shape, and increase in signal strength with layer thickness d_{CBP} until they saturate. In addition, the plasmonic resonance shifts toward lower energies with increasing layer thickness because of the change of the polarizability of the antennas' surrounding during evaporation. This shift is the base of localized surface plasmon resonance

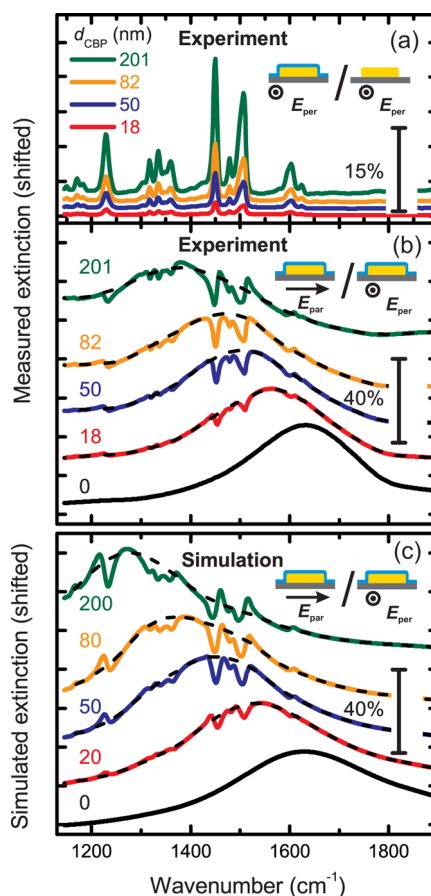


Figure 2. Measured (a and b) and simulated (c) extinction as deduced from the relative transmittance for selected thicknesses d_{CBP} given in nanometers (numbers, left). The inset (blue: CBP layer, orange: gold antennas, gray: substrate) indicates the respective normalization. (a) For thick layers several CBP vibrations are clearly visible in the spectra measured with light polarized perpendicular to the long wire axis and normalized to the bare substrate (see inset). (b) To obtain the antenna-enhanced signal originating solely from molecules located in the plasmonic near-fields, the ratio of parallel (E_{par}) and perpendicular (E_{per}) transmittance is calculated (see inset). Besides the broadband antenna resonance, which shifts with thickness, enhanced vibrational CBP signals increasing with thickness are observed. The black dashed lines in (b) and (c) represent fits to the bare antenna resonance curves. Please note the different scales in the respective panels.

sensing^{28,29} and is intrinsically connected with the vibrational signal enhancement, since both effects originate from the confined plasmonic near-fields.

We now compare our experimental results to numerical simulations (Figure 2c), which were carried out with the commercially available FDTD software package Lumerical. By solving Maxwell's equations, a numerical solution of the infrared transmittance for single antennas was obtained under normal incidence of a plane wave. The nanoantenna itself was modeled as a cuboid-like structure with dimensions taken from the fabrication process and covered with a homogeneous CBP layer of the respective thickness. The substrate beneath the gold antenna was described with a dispersionless refractive index of $n = 1.41$ without any

absorption. Furthermore, we described the infrared optical properties of gold with data by Palik.³⁰ The dielectric function of CBP was modeled as a sum of Brendel oscillators and a background polarizability of $\epsilon_\infty = 2.9$.²⁴ Further details are given in the Methods section. The numerically calculated infrared transmittance was processed analogous to our experimental data and is shown in Figure 2c for different layer thicknesses d_{CBP} . The simulated spectra are in very good qualitative agreement with the experimental ones. For example, the shift of the resonance frequency as well as the molecular signal evolution is well reproduced. However, there are also minor differences, mainly concerning the low energy range of our accessible spectrum. Here, the plasmonic resonance and also the signal enhancement of the C–H deformation vibration (mode at 1230 cm^{-1}) differ significantly. We attribute these differences to bulk multiphonon absorption of CaF_2 (onset at around 1000 cm^{-1}) and interaction effects between nanoantennas in the array (see Supporting Information), which are both not considered in the simulations due to computational restrictions. Depending on the periodicity of the antenna array, interferences may modify the plasmonic resonance (e.g., their line shape) as well as significantly influence the signal enhancement.⁹ In our experiments, a constructive interference is estimated to appear at approximately 1000 cm^{-1} , which is spectrally close to the resonance of nanoantennas covered with 200 nm of CBP. However, the spectral range between 1300 and 2000 cm^{-1} is not significantly impacted by the discussed issues, and vibrations located within this spectral range are therefore considered to be unaffected and included in our analysis. It should be mentioned that the dielectric background polarizability ($\epsilon_\infty \approx n_\infty^2$) of CBP, which predominantly determines the resonance position, contains an error of approximately 7%.²⁴ As we have evaluated with FDTD simulations of a nanoantenna covered with 150 nm of modified CBP ($n_\infty = 1.64$ instead of $n_\infty = 1.7$), such an error already causes a plasmon resonance shift of about 10%. This is an indicator of the high sensitivity of plasmonic resonances to refractive indices and, here, the explanation of some deviations between experimental and simulated resonance.

As a result of the plasmonic–molecular coupling, the molecular vibrations are enhanced, but inconveniently located on a nontrivial baseline given by the antenna resonance, which in addition changes with the CBP coverage. Thus, a reliable method for baseline correction is required. We used an adaption of the computational approach of asymmetric least-squares smoothing introduced by Eilers³¹ to fit our experimental and numerically calculated spectra. One advantage of the algorithm is the possibility to exclude data points from fitting, in our case the regions with vibrational signals. Following this approach, we obtained the

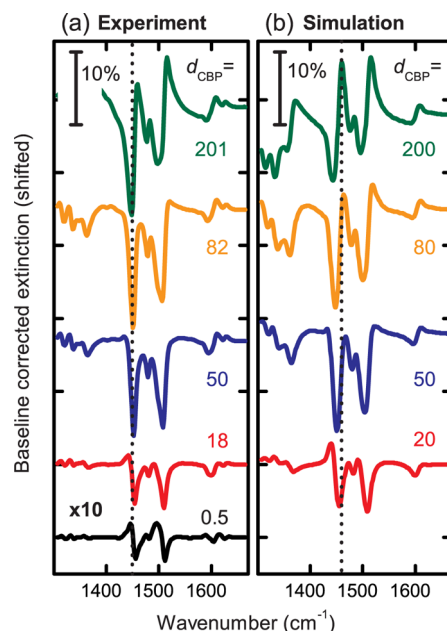


Figure 3. Plasmonically enhanced CBP vibrations after the baseline correction: experimental (a) and simulated (b) data. The vibrational Fano-type line shapes and signal strengths change with increasing CBP layer thickness (given in nanometers) that originates from a modified plasmon–molecule coupling induced by the polarizability of the evaporated material. For the sake of clarity, the black curve (CBP layer thickness of 0.5 nm) is multiplied by a factor of 10. The C–H deformation vibration (1450 cm^{-1}) is indicated by a dotted line and used for further analysis.

baseline-corrected extinction without any vibrational features (dashed black lines in Figure 2b and c). From this, we extracted the resonance frequencies (ω_{res}) and compared them to higher order excitations³² of the very same antenna and CBP thickness to evaluate the quality of the fitting. Furthermore, we performed FDTD simulations with a modified CBP model, only taking the dielectric background ϵ_∞ into account and thus neglecting the oscillators that describe the infrared vibrations. Both the comparison with higher order excitations and FDTD simulations provide very good agreement with the fitted resonance frequencies. Please note that the baseline correction is more reliable for weak molecular oscillators due to the negligible impact of the vibrations on the baseline.

A quantitative analysis of the signal evolution with layer thickness, however, requires full access to the asymmetric line shape of the enhanced vibrations, which we obtained by subtracting the fitted baseline from the experimental and simulated data, respectively. The corrected spectra (Figure 3) feature asymmetric molecular vibrations changing in intensity and line shape with increasing CBP coverage as a result of the coupling between the plasmonic and vibrational excitations.

It is known from the literature^{27,33,34} that the vibrational line shape follows a Fano-type behavior if the resonance frequency (ω_{res}) is shifted relatively to the

vibrational band (ω_{vib}). In these studies, ω_{res} was tuned via the antenna length, whereas in the present experiment the plasmonic resonance frequency and thus the tuning ratio (defined as $\omega_{\text{res}}/\omega_{\text{vib}}$) is changed due to the increased polarizability of the evaporated material. For the thinnest layer thickness of only 0.5 nm we already observe enhanced molecular vibrations (black curve), which increase for thicker layers, since more CBP is located in the plasmonic near-fields. On the other hand, the signal enhancement also changes with the resonance frequency, which hampers a direct comparison of the molecular vibrations of different layer thicknesses. In the simulated spectra, for example, the enhanced C–C stretching vibration (1600 cm^{-1}) of the 20 nm thick layer (red curve) shows a signal strength comparable to the 50 nm one (blue curve), even though the amount of material is twice as much. In order to separate the undesired influence of the tuning from the impact of the layer thickness on the signal evolution, we prepared a second series of nanoantennas with various lengths having resonances close to the CBP vibrations. After the nanostructures were covered with a 5 nm thick CBP layer, infrared spectroscopy was conducted and the tuning dependence of the C–H deformation vibration was evaluated.²⁶ By fitting a driven harmonic oscillator, we finally obtain a calibration curve (Figure S2a) reaching its maximum close to a perfect match of the plasmonic and vibrational excitation. This result is expected^{35,36} and used to correct for the tuning in our experiments (see Supporting Information). Certainly, the origin of the resonance shift differs in both kinds of studies. Whereas in our reference measurements the plasmon changes with length, the resonance shift is caused by the polarizability of the evaporated CBP material in the other experiment. With FDTD simulations we proved that the near-field distribution is only marginally affected by the evaporated material, justifying the above-mentioned approximation (see Supporting Information).

For a more detailed analysis of the signal evolution with layer thickness we representatively consider the C–H deformation vibration at 1450 cm^{-1} . Its vibrational strength, defined as the difference between minimum and maximum, is extracted from the baseline-corrected spectra (Figure 3) and corrected for the tuning as described above. As a result, we obtain the enhanced signal strengths (open symbols) with respect to the CBP layer thickness (Figure 4).

For a low CBP coverage we observe a steep increase of the enhanced signal strength, which then saturates for thicker layers. Please note that the signal originates only from molecules located in the plasmonic near-fields (compare Figure 2). The behavior is expected from the electromagnetic near-field of the resonantly excited antenna (see Figure 1b), which rapidly decreases with increasing distance from the antenna

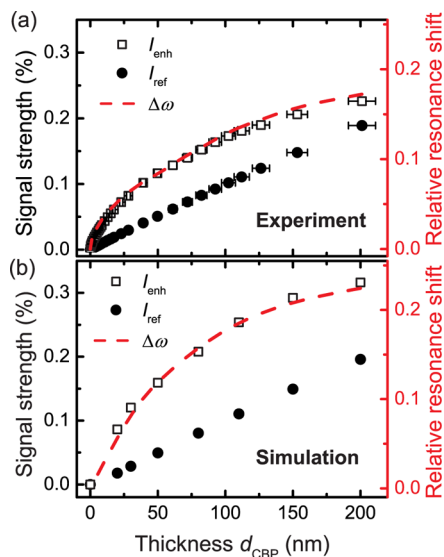


Figure 4. Evolution of signal strength with layer thickness for the plasmonically enhanced (I_{enh} , open squares) and unenhanced (I_{ref} , filled dots) C–H deformation vibration (1450 cm^{-1}). As expected, the enhanced vibrational signal saturates for thicker layers, whereas the unenhanced signal increases linearly. The relative resonance shift (red dashed line) is defined as $\Delta\omega = (\omega_{\text{res}}(d_{\text{CBP}}) - \omega_{\text{res}}(0))/\omega_{\text{res}}(0)$, where $\omega_{\text{res}}(d_{\text{CBP}})$ is the resonance frequency at the respective thickness d_{CBP} . It evolves similarly to the enhanced vibrational signal. The data extracted from simulations (b) are in good qualitative agreement with the measurements (a).

surface. Since the enhanced signal strength scales with the plasmonic near-fields,¹⁴ vibrations of molecules located in the direct vicinity of the nanoantenna are strongly enhanced, while vibrations of molecules located apart do not contribute significantly to the integrated signal. For this reason a constant signal is expected in the limit of infinite distances. In contrast, the unenhanced signal strength (filled dots) measured in perpendicular polarization (see spectra in Figure 2a) linearly increases with the layer thickness only as expected from Lambert–Beer’s law. Interestingly, for a thickness of about 250 nm the enhanced and unenhanced signal strengths are similar. This means that antenna-assisted SEIRA provides higher sensitivity only in comparison to conventional infrared spectroscopy below this value for the given molecular–plasmonic system, which is in agreement with previous numerical studies.¹⁹ Finally, the relative resonance shift $\Delta\omega_{\text{res}}$ (red dashed line) behaves very similarly with respect to the enhanced signal, indicating that the resonance shift as well as the enhanced vibration is very distance dependent. Please note that the enhanced signal is already corrected for different plasmonic–vibrational coupling strengths caused by different tuning ratios (see Supporting Information). The identical feature of the two curves, however, further reveals the same nature of the shift and signal enhancement, which is the confined electromagnetic near-field of the antenna.

The experimental findings are in good qualitative agreement with the numerically calculated data. In line

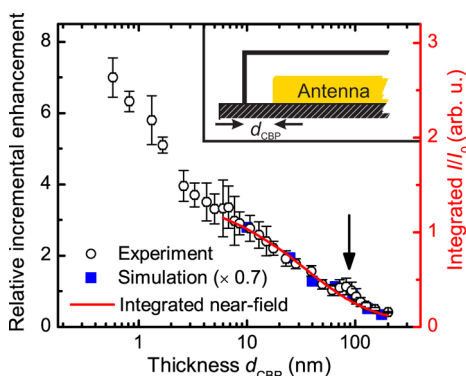


Figure 5. Relative incremental enhancement ($dI_{\text{enh}}/dd_{\text{CBP}}$) ($dI_{\text{ref}}/dd_{\text{CBP}}$) at a certain distance d_{CBP} from the antenna (the quotient of the derivatives of the enhanced ($dI_{\text{enh}}/dd_{\text{CBP}}$) and unenhanced ($dI_{\text{ref}}/dd_{\text{CBP}}$) for the C–H deformation vibration ($\omega_{\text{vib}} = 1450 \text{ cm}^{-1}$) versus the layer thickness d_{CBP} . The simulated (blue symbols) data are normalized to the experimental ones (black symbols). The red curve represents the numerically calculated near-field intensity enhancement I/I_0 summed up over the surfaces of a cuboid defined by the antennas' geometry and the respective layer thickness at certain distance d_{CBP} (see inset). The inset depicts a cross-section, where the surface of the cuboid surface is sketched as a black line. The dashed area indicates the substrate. A good qualitative agreement between the decay of I/I_0 and of the simulated and experimental increments is found from about 5 nm on with slight deviations around 80 nm (indicated by the black arrow).

with our experimental results, we observe saturation of the enhanced signal strength as well as the relative resonance shift. There are quantitative differences with respect to the frequency shift and the enhanced signal strength that mainly originate from the modeling of the nanostructures (e.g. as ideal arrangement on a nonabsorbing substrate) and the CBP layer (as a completely smooth one with a background polarizability from literature) in our simulations as addressed above.

In our study, we always measure an integrated signal strength also containing the contributions of the molecules from lower layers. In order to determine the contribution of the enhanced signal at a certain distance to the integrated signal strength only, we calculate the derivative of the enhanced ($dI_{\text{enh}}/dd_{\text{CBP}}$) and unenhanced signal ($dI_{\text{ref}}/dd_{\text{CBP}}$) with thickness. Building the quotient of both derivatives yields the relative incremental enhancement at a certain distance (thickness in Figure 5), which is a measure of the enhanced electromagnetic near-field at this distance.

For coverage above approximately 5 nm the experimental incremental enhancement is in good qualitative agreement with the decay of the simulated one (blue symbols; for better comparison of the slope, data from simulation are normalized to experimental data at $d_{\text{CBP}} = 10 \text{ nm}$). In order to address the relation between the incremental enhancement and the near-field, we summed up the numerically calculated near-field intensity I/I_0 (compare Figure 1b) over the surfaces of a cuboid defined by the antenna geometry and the respective layer thickness at certain distance d_{CBP}

located symmetrically around the antenna (see inset in Figure 5). The identical decay of both curves proves the purely electromagnetic nature of the SEIRA enhancement mechanism and confirms that the antenna-enhanced signal strengths linearly scale with the near-field intensity as suggested by previous studies.¹⁴ Obviously, at a thickness of about 80 nm, corresponding to the antenna height, the simulated intensity slightly differs from the experimental incremental (see black arrow). In contrast to our assumption in the near-field simulations (red curve), the CBP layer also grows on the CaF_2 substrate and not solely around the nanostructure. Thus, molecules located at distances larger than 80 nm also contribute to the enhanced signal (even though the contribution is very small). This situation in combination with more intense electromagnetic near-fields at the upper antenna surface (Figure 1b) leads to an enlarged relative incremental enhancement in comparison to our near-field simulations. The tiny feature at 80 nm demonstrates the sensitivity of the measurement to the morphology of the molecular layer on the substrate in the vicinity of the antenna. Also in the coverage regime below 5 nm the morphology of the evaporated film may play a crucial role. More specifically, the stochastic nature of the evaporation process always yields condensation nuclei. The evaporation on gold at room temperature enables only limited molecular diffusion, resulting in a disturbed layer-by-layer growth where more molecules stick at higher layers before lower ones are completed. Consequently, the incremental signal enhancement may decrease more rapidly, as observed below 5 nm, than for thicker layers, where the film entirely covers the surface, as we prove by atomic force microscopy (AFM, see Supporting Information). Inconveniently, this low thickness range is not accessible with our purely electromagnetic simulations due computational and, below 1 nm, conceptual limitations, e.g., nonlocal and quantum effects.¹¹ Also, the molecules are not small enough for even higher resolution at even smaller distances.

Finally, we representatively estimated an enhancement factor for a layer thickness of one nanometer. Therefore, we multiply the ratio (approximately 6) of the enhanced (Figure 5a, open squares) and unenhanced (Figure 5a, filled dots) signal taken at a distance of one nanometer with the relative fraction of molecules actively contributing to the signal. In our reference experiments (perpendicular polarization) the ratio is 1, since all adsorbed molecules are measured, whereas in the SEIRA studies (parallel polarization) only the molecules located in the plasmonic near-fields contribute to the signal. Assuming homogeneous CBP coverage and an active area of two times the antenna end faces according to ref 12, we deduce enhancement factors of up to 25 000, in agreement with other studies.²⁶

CONCLUSION

In summary, molecular layers of CBP are utilized to probe the distance dependence of antenna-assisted SEIRA with nanometer-scale resolution up to more than 200 nm in distance. In good qualitative agreement with our numerical calculations we experimentally observed a decrease of the signal enhancement with probe layer thickness originating from the rapidly decaying electromagnetic near-fields of resonantly excited nanostructures. The highest sensitivity is found for the thinnest layers due to the strongly confined nature of the electromagnetic near-field. From about 5 nm on, the relative incremental enhancement of IR vibrations linearly scales with the near-field intensity, as we have proven in this study. Thus, for the distance range beyond 5 nm, our approach is also applicable to

gain precise information on the near-field of plasmonic nanostructures of any shape as well as their expected SEIRA enhancement.

With respect to possible sensor concepts based on antenna-assisted SEIRA, the signal evolution with layer thickness is most important. A comparison of the enhanced signal to the unenhanced one reveals that antenna-enhanced spectroscopy provides higher sensitivity only with respect to conventional infrared spectroscopy below 250 nm layer thickness for the given molecular–plasmonic system. The onset of saturation of SEIRA effectively starts already at about 100 nm thickness, beyond which the signal enhancement is negligibly small. Consequently, several hundred nanometer-sized objects such as bacteria or cells can be studied with SEIRA of surface regions, which may be of interest for membrane studies.

METHODS

Nanofabrication. The nanoantenna array was defined on an infrared-transparent calcium difluoride (CaF_2) substrate (purchased from CrysTec GmbH, Berlin) via standard electron beam lithography (Raith eLine) in double-layer PMMA resist (poly(methyl methacrylate), 250 K, 2.5% and 950 K 1.5%, Allresist). After development in MIBK (methyl isobutyl ketone, diluted 1:5 in 2-propanol) a 2 nm chromium adhesion layer and an 80 nm gold film are thermally evaporated followed by a lift-off procedure (commercial remover based on NEP (*N*-ethyl-2-pyrrolidone), Allresist, 65 °C, 2 h). The final nanoantenna array dimensions are antenna length $L = 2140$ nm, width $w = 90$ nm, and height $h = 80$ nm, periodicity $p_x = 3140$ nm and $p_y = 8090$ nm, and array size of 5×5 mm².

Infrared Spectroscopy and Molecular Evaporation. The organic material 4,4'-bis(*N*-carbazolyl)-1,1'-biphenyl (CBP) was purchased from Sigma-Aldrich with a purity of 99.9% and used without any further purification. It was evaporated on the nanostructure sample employing resistively heated quartz crucibles in a UHV chamber. The deposition rates were controlled by a quartz-crystal microbalance and were kept at 0.5 nm/min for layer thicknesses up to 20 nm and approximately 1 nm/min for layer thicknesses between 20 and 200 nm. The UHV chamber was connected to a Fourier-transform infrared spectrometer. By means of mirror optics the infrared beam was coupled into the chamber, sent through a KRS-5 polarizer, and focused on the sample (spot size of approximately 3 mm). After passing the nanostructure sample, the transmitted infrared radiation was detected with a mercury-cadmium-telluride (MCT) detector located outside the UHV chamber. The base pressure during sample preparation and spectroscopic measurements was 3×10^{-9} mbar in the UHV chamber and 3 mbar in the spectrometer and detector housing to prevent atmospheric absorption. The transmission spectra were recorded directly after CBP deposition with a resolution of 4 cm⁻¹ and at least 500 scans at room temperature. After each evaporation step, corresponding to a certain layer thickness, spectra with polarization parallel and perpendicular to the long antenna axis were acquired subsequently without moving the sample. Thus, infrared spectroscopic measurements at the very same position and the same layer thickness were assured for both polarizations.

Numerical Simulations. Near-field distributions and far-field infrared transmittance were calculated using the commercial FDTD software Lumerical FDTD-Solutions v8.5.3. The infrared transmittance of individual nanoantennas was obtained by numerically solving Maxwell's equations under normal incidence of infrared radiation polarized parallel and perpendicular to the long antenna axis. In all simulations, the antenna was

placed on a CaF_2 substrate and is situated at least one wavelength size away from the perfect matched layers (PMLs) that describe the boundary conditions of the simulation volume. The CBP coverage of the substrate and the nanostructure with different thickness d_{CBP} was assumed to be homogeneous, as depicted in Figure 1a. In a first approximation, CaF_2 was described by a dispersionless refractive index of $n = 1.41$, the optical data of gold were taken from Palik,³⁰ and the dielectric function of CBP was taken from ref 24. Dielectric functions of both CBP and gold were fitted with a built-in multicoefficient model employing 40 and 2 coefficients, respectively. In order to resolve the nanometer thickness of the molecular layer, sub-gridding techniques were employed to obtain mesh cell sizes down to $3 \times 3 \times 3$ nm in volume given by the antenna and CBP layer. Mesh sizes smaller than 100 nm were used elsewhere. A plane wave incident from a broadband source (1000 to 2000 cm⁻¹) located inside the CaF_2 substrate excited the nanostructure. Its transmittance was calculated by integrating the power flux through a power monitor situated in air and normalizing it with respect to the source power. Electromagnetic field strengths of resonantly excited antennas without any CBP (Figure 1b), however, were recorded with a two-dimensional field profile monitor placed normal to the substrate and parallel to the long wire axis. To avoid any simulation artifacts, the electromagnetic field was taken 6 nm above the antenna surface. Convergence testing was performed by iteratively increasing the simulation volume, the number of PMLs, and simulation times (up to 1×10^{-11} s) as well as reducing the mesh sizes until the results converged. Typical residual energies of the decayed electromagnetic fields below 1×10^{-8} were found at the end of simulations. All symmetries provided by the nanostructures were included in the simulation setup to reduce the computational requirements.

Analytical Calculations. For determining the layer thickness the commercially available software package SCOUT 3.62 (W. Theiss, hard- and software) was used. In SCOUT relative transmission spectra of defined layer stacks are calculated using the transfer-matrix method. Each material in a layer stack is represented by its dielectric function consisting of a dielectric background and several Brendel oscillators, which account for the different vibrational modes of the material.

Conflict of Interest: The authors declare no competing financial interest.

Acknowledgment. The authors from the University Stuttgart acknowledge financial support by the Baden-Württemberg Stiftung and the ERC (COMPLEXPLAS). We are grateful for computational resources provided by the bwGRID of the federal

state of Baden-Württemberg, Germany. The authors from University of Heidelberg acknowledge financial support from BMBF via the MESOMERIE Project (FKZ 13N10724). S.B. also acknowledges support from the Heidelberg Graduate School for Fundamental Physics (HGSFP). We additionally would like to thank C. Huck, J. Vogt, J. Bochterle, and D. Dregely for their discussions and comments and M. Scherer for the supply of AFM measurements.

Supporting Information Available: Evaporation of CBP on unstructured silicon wafers and IR spectra. Tuning dependency of antenna-enhanced vibrational signals. Atomic force microscopic studies of CBP on gold. FDTD simulations of two-dimensional antenna arrays. This material is available free of charge via the Internet at <http://pubs.acs.org>.

REFERENCES AND NOTES

- Osawa, M.; Ataka, K.-I.; Yoshii, K.; Nishikawa, Y. Surface-Enhanced Infrared Spectroscopy: The Origin of the Absorption Enhancement and Band Selection Rule in the Infrared Spectra of Molecules Adsorbed on Fine Metal Particles. *Appl. Spectrosc.* **1993**, *47*, 1497–1502.
- Neubrech, F.; Pucci, A. Plasmonic Enhancement of Vibrational Excitations in the Infrared. *IEEE J. Sel. Top. Quant.* **2013**, *19*, 4600809.
- Neubrech, F.; Pucci, A.; Cornelius, T. W.; Karim, S.; Garcia-Etxarri, A.; Aizpurua, J. Resonant Plasmonic and Vibrational Coupling in a Tailored Nanoantenna for Infrared Detection. *Phys. Rev. Lett.* **2008**, *101*, 157403.
- Pryce, I. M.; Kelaita, Y. A.; Aydin, K.; Atwater, H. A. Compliant Metamaterials for Resonantly Enhanced Infrared Absorption Spectroscopy and Refractive Index Sensing. *ACS Nano* **2011**, *5*, 8167–8174.
- Cubukcu, E.; Zhang, S.; Park, Y.-S.; Bartal, G.; Zhang, X. Split Ring Resonator Sensors for Infrared Detection of Single Molecular Monolayers. *Appl. Phys. Lett.* **2009**, *95*, 043113.
- Aouani, H.; Rahmani, M.; Sipova, H.; Torres, V.; Hegnerova, K.; Beruete, M.; Homola, J.; Hong, M.; Navarro-Cia, M.; Maier, S. A. Plasmonic Nanoantennas for Multispectral Surface-Enhanced Spectroscopies. *J. Phys. Chem. C* **2013**, *117*, 18620–18626.
- Le, F.; Brandl, D. W.; Urzhumov, Y. A.; Wang, H.; Kundu, J.; Halas, N. J.; Aizpurua, J.; Nordlander, P. Metallic Nanoparticle Arrays: A Common Substrate for Both Surface-Enhanced Raman Scattering and Surface-Enhanced Infrared Absorption. *ACS Nano* **2008**, *2*, 707–718.
- Adato, R.; Altug, H. *In-Situ* Ultra-Sensitive Infrared Absorption Spectroscopy of Biomolecule Interactions in Real Time with Plasmonic Nanoantennas. *Nat. Commun.* **2013**, *4*, 2154.
- Adato, R.; Yanik, A. A.; Amsden, J. J.; Kaplan, D. L.; Omenetto, F. G.; Hong, M. K.; Erramilli, S.; Altug, H. Ultra-Sensitive Vibrational Spectroscopy of Protein Monolayers with Plasmonic Nanoantenna Arrays. *Proc. Natl. Acad. Sci. U.S.A.* **2009**, *106*, 19227–19232.
- Srajer, J.; Schwaighofer, A.; Ramer, G.; Rotter, S.; Guenay, B.; Kriegner, A.; Knoll, W.; Lendl, B.; Nowak, C. Double-Layered Nanoparticle Stacks for Surface-Enhanced Infrared Absorption Spectroscopy. *Nanoscale* **2014**, *6*, 127–131.
- Zuloaga, J.; Prodan, E.; Nordlander, P. Quantum Plasmonics: Optical Properties and Tunability of Metallic Nanorods. *ACS Nano* **2010**, *4*, 5269–5276.
- Bochterle, J.; Neubrech, F.; Nagao, T.; Pucci, A. Angstrom-Scale Distance Dependence of Antenna-Enhanced Vibrational Signals. *ACS Nano* **2012**, *6*, 10917–10923.
- Brown, L. V.; Zhao, K.; King, N.; Sobhani, H.; Nordlander, P.; Halas, N. J. Surface-Enhanced Infrared Absorption Using Individual Cross Antennas Tailored to Chemical Moieties. *J. Am. Chem. Soc.* **2013**, *135*, 3688–3695.
- Dregely, D.; Neubrech, F.; Duan, H.; Vogelgesang, R.; Giessen, H. Vibrational Near-Field Mapping of Planar and Buried Three-Dimensional Plasmonic Nanostructures. *Nat. Commun.* **2013**, *4*, 2237.
- Gallinet, B.; Martin, O. J. F. Ab Initio Theory of Fano Resonances in Plasmonic Nanostructures and Metamaterials. *Phys. Rev. B* **2011**, *83*, 235427.
- Ataka, K.; Stripp, S. T.; Heberle, J. Surface-Enhanced Infrared Absorption Spectroscopy (SEIRAS) to Probe Monolayers of Membrane Proteins. *Biochim. Biophys. Acta, Biomembr.* **2013**, *1828*, 2283–2293.
- Hoffmann, J. M.; Yin, X.; Richter, J.; Hartung, A.; Ma, T. W. W.; Taubner, T. Low-Cost Infrared Resonant Structures for Surface-Enhanced Infrared Absorption Spectroscopy in the Fingerprint Region from 3 to 13 μm . *J. Phys. Chem. C* **2013**, *117*, 11311–11316.
- Cetin, A. E.; Altug, H. Fano Resonant Ring/Disk Plasmonic Nanocavities on Conducting Substrates for Advanced Biosensing. *ACS Nano* **2012**, *6*, 9989–9995.
- Lieberman, V.; Adato, R.; Jeys, T. H.; Saar, B. G.; Erramilli, S.; Altug, H. Rational Design and Optimization of Plasmonic Nanoarrays for Surface-Enhanced Infrared Spectroscopy. *Opt. Express* **2012**, *20*, 11953–11967.
- Aizpurua, J.; Bryant, G. W.; Richter, L. J.; Garc de Abajo, F. J.; Kelley, B. K.; Mallouk, T. Optical Properties of Coupled Metallic Nanorods for Field-Enhanced Spectroscopy. *Phys. Rev. B* **2005**, *71*, 235420.
- Schumacher, T.; Kratzer, K.; Molnar, D.; Hentschel, M.; Giessen, H.; Lippitz, M. Nanoantenna-Enhanced Ultrafast Nonlinear Spectroscopy of a Single Gold Nanoparticle. *Nat. Commun.* **2011**, *2*, 333.
- Schnell, M.; Garcia-Etxarri, A.; Huber, J. A.; Crozier, K.; Aizpurua, J.; Hillenbrand, R. Controlling the Near-Field Oscillations of Loaded Plasmonic Nanoantennas. *Nat. Photonics* **2009**, *3*, 287–291.
- Olmon, R. L.; Krenz, P. M.; Jones, A. C.; Boreman, G. D.; Raschke, M. B. Near-Field Imaging of Optical Antenna Modes in the Mid-Infrared. *Opt. Express* **2008**, *16*, 20295–20305.
- Glaser, T.; Beck, S.; Lunkenheimer, B.; Donhauser, D.; Köhn, A.; Kröger, M.; Pucci, A. Infrared Study of the MoO₃ Doping Efficiency in 4,4'-Bis(N-Carbazolyl)-1,1'-Biphenyl (CBP). *Org. Electron.* **2013**, *14*, 575–583.
- Yu, X.; Cai, H.; Zhang, W.; Li, X.; Pan, N.; Luo, Y.; Wang, X.; Hou, J. G. Tuning Chemical Enhancement of SERS by Controlling the Chemical Reduction of Graphene Oxide Nanosheets. *ACS Nano* **2011**, *5*, 952–958.
- Huck, C.; Neubrech, F.; Vogt, J.; Toma, A.; Gerbert, D.; Katzmann, J.; Härtling, T.; Pucci, A. Surface-Enhanced Infrared Spectroscopy Using Nanometer-Sized Gaps. *ACS Nano* **2014**, *10*, 1021/nn500903v.
- Giannini, V.; Francescato, Y.; Amrania, H.; Phillips, C. C.; Maier, S. A. Fano Resonances in Nanoscale Plasmonic Systems: A Parameter-Free Modeling Approach. *Nano Lett.* **2011**, *11*, 2835–2840.
- Svedendahl, M.; Chen, S.; Dmitriev, A.; Käll, M. Refractometric Sensing Using Propagating versus Localized Surface Plasmons: A Direct Comparison. *Nano Lett.* **2009**, *9*, 4428–4433.
- Ament, I.; Prasad, J.; Henkel, A.; Schmachtel, S.; Sönnichsen, C. Single Unlabeled Protein Detection on Individual Plasmonic Nanoparticles. *Nano Lett.* **2012**, *12*, 1092–1095.
- Palik, E. D. *Handbook of Optical Constants of Solids*; Academic Press: New York, 1985.
- Eilers, P. H. C. A Perfect Smoother. *Anal. Chem.* **2003**, *75*, 3631–3636.
- Novotny, L. Effective Wavelength Scaling for Optical Antennas. *Phys. Rev. Lett.* **2007**, *98*, 266802.
- Osley, E. J.; Biris, C. G.; Thompson, P. G.; Jahromi, R. R. F.; Warburton, P. A.; Panoui, N. C. Fano Resonance Resulting from a Tunable Interaction between Molecular Vibrational Modes and a Double Continuum of a Plasmonic Molecule. *Phys. Rev. Lett.* **2013**, *110*, 087402.
- Abb, M.; Wang, Y.; Papisimakis, N.; de Groot, C. H.; Muskens, O. L. Surface-Enhanced Infrared Spectroscopy Using Metal Oxide Plasmonic Antenna Arrays. *Nano Lett.* **2013**, *14*, 346–352.
- Zuloaga, J.; Nordlander, P. On the Energy Shift between Near-Field and Far-Field Peak Intensities in Localized Plasmon Systems. *Nano Lett.* **2011**, *11*, 1280–1283.

36. Alonso-Gonzalez, P.; Albella, P.; Neubrech, F.; Huck, C.; Chen, J.; Golmar, F.; Casanova, F.; Hueso, L. E.; Pucci, A.; Aizpurua, J.; Hillenbrand, R. Experimental Verification of the Spectral Shift between Near- and Far-Field Peak Intensities of Plasmonic Infrared Nanoantennas. *Phys. Rev. Lett.* **2013**, *110*, 203902.